Antoranz, A.; Gonzalo, A.; Flores, O.; García-Villalba, M. (2015). Numerical simulation of heat transfer in a pipe with non-homogeneous thermal boundary conditions. *International Journal of Heat and Fluid Flow*, volume 55, pages 45–51.
doi: 10.1016/j.ijheatfluidflow.2015.05.007

Numerical simulation of heat transfer in a pipe with non-homogeneous thermal boundary conditions

A. Antoranz[a,b], A. Gonzalo[a], O. Flores[a], M. García-Villalba[a]

[a]*Bioingeniería e Ing. Aeroespacial, Universidad Carlos III de Madrid, 28911 Leganés, Spain*
[b]*Industria de Turbopropulsores (ITP)*

Abstract

Direct numerical simulations of heat transfer in a fully-developed turbulent pipe flow with circumferentially-varying thermal boundary conditions are reported. Three cases have been considered for friction Reynolds number in the range 180–360 and Prandtl number in the range 0.7–4. The temperature statistics under these heating conditions are characterized. Eddy diffusivities and turbulent Prandtl numbers for radial and circumferential directions are evaluated and compared to the values predicted by simple models. It is found that the usual assumptions made in these models provide reasonable predictions far from the wall and that corrections to the models are needed near the wall.

Keywords: direct numerical simulation, heat transfer, pipe flow, turbulence, eddy-diffusivity

1. Introduction

Prediction of turbulent flows characterized by large temperature gradients and high heat-transfer rates is of great importance in engineering. Heat exchangers, combustion chambers, nuclear reactors and cooling systems in electronic devices are just some of the well-known examples in which significant temperature variations typically occur within the flow. In particular, the motivation for this study is the flow in the tubes of the heat receiver of concentrated solar power towers (Moore et al., 2010; Kolb, 2011). The heat receivers are formed by thin-walled metal tubes, assembled into panels. Heliostats located around the tower concentrate the solar radiation onto the tubes. Since the tubes are irradiated only on their outward facing side, they are subject to highly non-uniform heat flux. The heat transfer fluid, typically a molten nitrate salt, flows through the tubes increasing its temperature by convection. From a design point of view, the problem is complicated since the density, the viscosity and the heat conductivity of the salts are temperature dependent. Although the Reynolds numbers of operation are not extremely large, in the

Email address: antonio.antoranz@uc3m.es (A. Antoranz)

Case	Re_τ	Re_b	Pr	Line style
1	180	$5.26 \cdot 10^3$	0.7	Solid (Black online)
2	180	$5.26 \cdot 10^3$	4	Dashed (Red online)
3	360	$1.16 \cdot 10^4$	0.7	Dashed-dotted (Blue online)

Table 1: Parameters of the simulations. $Re_\tau = u_\tau R/\nu$, $Re_b = U_b 2R/\nu$, where R is the pipe radius, u_τ is the friction velocity, U_b is the bulk velocity and ν is the kinematic viscosity.

range $Re_b = 2U_bR/\nu = 2 \cdot 10^4$ – $4 \cdot 10^4$, where U_b is the bulk velocity, R is the pipe radius and ν is the kinematic viscosity, the Prandtl numbers are large, in the range 10–20 depending on the employed salt. The operation of the plant must ensure that the temperature of the salt never reaches the decomposition temperature nor the melting temperature. This is not always easy to predict and requires a greater understanding of the temperature distribution than currently available. Such understanding may be obtained through direct numerical simulations (DNS) of fully developed turbulent flow in pipes. These simulations are becoming affordable with the recent advances in computational power, specially for the lower end of the range of Reynolds and Prandtl numbers mentioned above.

In spite of its practical relevance, turbulent heat transfer in pipes has not been so thoroughly studied through DNS as in plane channel flows. The main reason is the numerical difficulties associated with the cylindrical coordinate system and the corresponding numerical singularity along the symmetry line. There are some DNS of turbulent pipe flow without heat transfer like those of Wu and Moin (2008), El Khoury et al. (2013) and Chin et al. (2014). DNS of heat transfer in pipes with *homogeneous* heating are also available, for example Piller (2005) and Redjem-Saad et al. (2007). To the best of our knowledge DNS of pipe flow with *circumferentially-varying* heat flux are not available in the literature.

In this paper we report on the turbulent heat transfer in a pipe with circumferentially-varying heat flux by means of DNS of fully-developed turbulent flow. As a first step towards understanding the heat transfer characteristics of the pipes used in heat receivers, we simplify the problem by considering constant fluid properties and somewhat lower Reynolds and Prandtl numbers, as summarized in Table 1.

The main objective of the study is to generate a numerical database for RANS turbulence models benchmarking. We are particularly interested in the improvement of eddy diffusivity models, since there is a need to use very simplified models in some practical applications as the preliminary design of the heat receivers of concentrated solar power towers (Flores et al., 2014).

From experimental studies it is clear that the effective thermal diffusivity in a circular pipe is significantly non-isotropic, being higher in the circumferential than in the radial direction, as reported for example by the experiments of Quarmby and Quirk (1972). Besides this empirical evidence, many RANS calculations of the turbulent heat-transfer still use isotropic models for the thermal eddy-diffusivity as

the one employed by Reynolds (1963). Gärtner et al. (1974) improved on Reynolds results by employing a non-isotropic model. Later, Launder (1978) suggested that, for an axisymmetric fully-developed velocity field, the ratio of circumferential-to-radial heat eddy diffusivities can be approximated by the ratio of the corresponding mean square velocity fluctuations. Baughn et al. (1984) applied this model to the case of a pipe with a top-half heating distribution (constant heat flux on one half of the circunference but adiabatic conditions on the other half) obtaining remarkable better results that when using an isotropic eddy diffusivity model. The DNS database reported in this paper will allow to assess the accuracy and validity of such models.

The structure of the paper is as follows. In section 2 the computational setup is presented, including the governing equations and the boundary conditions. Results are presented in section 3. First, the temperature statistics are characterized. This is followed by the evaluation of eddy diffusivities and turbulent Prandtl numbers. Finally, conclusions are presented in section 4.

2. Governing equations and computational setup

As discussed in the introduction, the flow configuration studied in the present paper is a pressure-driven incompressible flow of a viscous fluid in a smooth circular pipe of radius R, subjected to a circumferentially-varying heat flux. The fluid has constant density, ρ, kinematic viscosity, ν, thermal diffusivity, α, and specific heat, C_p. Since gravity effects are not considered in the present study, the fluid temperature is simply treated as a passive scalar. Hence, the system of equations that need to be solved are the Navier-Stokes equations for an incompressible fluid (continuity and momentum), together with an advection-difussion equation for the temperature.

In the following the nomenclature used is (x_1, x_2, x_3) for the three cartesian coordinates, with corresponding velocity components (u_1, u_2, u_3). Due to the geometry of the problem, it is convenient to define also cylindrical coordinates (r, θ, z) and velocities (u_r, u_θ, u_z), where $z = x_3$ is the axial coordinate along the pipe axis (see Fig. 1). Several averages will be used throughout the paper. The brackets $\langle\cdot\rangle$ indicate mean values, averaged in time and over the homogeneous directions. Primed variables denote fluctuations with respect to these mean values. Bulk variables, denoted with a b subindex, are averaged in time and over the cross-plane (r, θ).

The boundary conditions imposed at the wall are no-slip for the velocity and a circumferentially-varying heat flux given by

$$q_w(\theta) = \pi \overline{q}_w \sin\theta, \qquad 0 < \theta < \pi \tag{1}$$

$$q_w(\theta) = 0, \qquad \pi < \theta < 2\pi \tag{2}$$

where $\overline{q}_w$ is the net heat flux at the wall, which corresponds to the value of the heat flux in a homogeneous heating case with the same total added heat to the system.

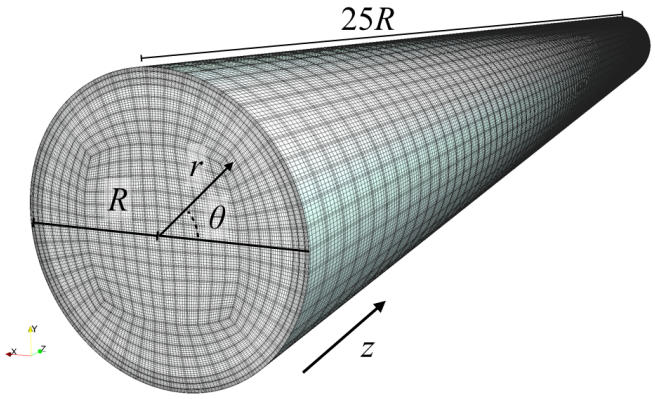

Figure 1: Computational domain and mesh.

The imposed heat flux aims to reproduce the heat transfer conditions of the pipes in a heat receiver, where the sun radiation only affects half of the circumference, while the other half can be considered adiabatic. Note that the added heat leads to a net increase of the temperature along the axial direction. A heat balance in a thin slab shows that the bulk temperature T_b increases linearly with z, with a slope given by

$$\frac{\mathrm{d}T_b}{\mathrm{d}z} = \frac{2\overline{q}_w}{\rho C_p U_b R}, \tag{3}$$

where U_b is the bulk velocity.

The net heat flux $\overline{q}_w$, together with the friction velocity, u_τ, allows the definition of a characteristic friction temperature $T^* = \overline{q}_w/\rho C_p u_\tau$. When the equations are normalised using the pipe radius R, the friction velocity u_τ and the friction temperature T^*, the only non-dimensional parameters that control the heat transfer are the Reynolds number $Re_\tau = u_\tau R/\nu$ and the Prandtl number $Pr = \nu/\alpha$. Three cases are defined with the values of Re_τ and Pr summarized in Table 1.

The linear increase of T_b with z allows us to simplify the advection-diffusion equation for the temperature, by decomposing the temperature field into $T_b(z) + T(r, \theta, z, t)$. The evolution equation for the latter is

$$\frac{\partial T}{\partial t} + u_i \frac{\partial T}{\partial x_i} = \alpha \frac{\partial^2 T}{\partial x_i \partial x_i} - u_3 \frac{\mathrm{d}T_b}{\mathrm{d}z}, \tag{4}$$

where the last term acts as a source term. Note that, since dT_b/dz is constant, the axial direction is homogeneous for $T(r, \theta, z, t)$.

Equation (4), together with the continuity and momentun equations, are solved using the massively parallel spectral-element method (SEM) solver Nek5000. This

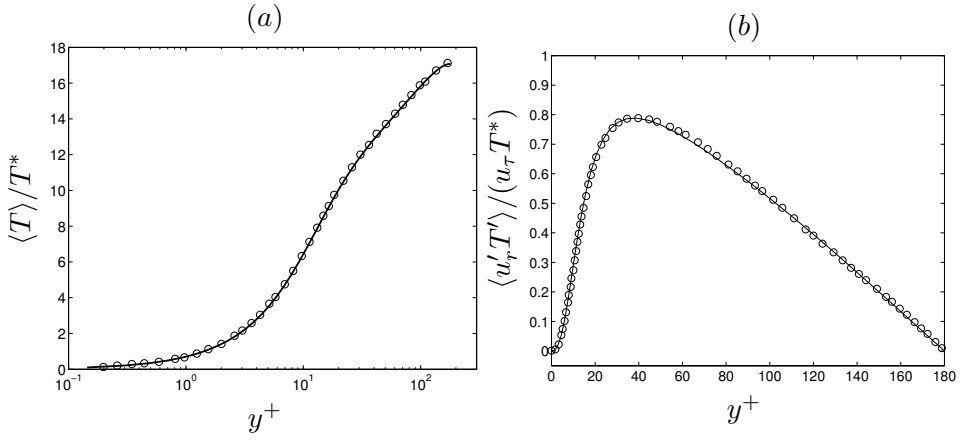

Figure 2: Results for the uniform heat flux case. Lines, present calculation. Symbols, data from Piller (2005). (a) Mean temperature $\langle T\rangle/T^*$ as a function to the distance to the wall $y^+ = (R-r)u_\tau/\nu$. (b) Turbulent heat flux $\langle u_r'T'\rangle/(u_\tau T^*)$ vs y^+.

code has been developed by Fischer et al. (2008), and it solves the incompressible Navier-Stokes equations on Gauss-Lobatto-Legendre nodes. It essentially divides the physical domain into a number of hexahedral elements where the equations of motion are solved by means of local approximations based on high-order orthogonal polynomials basis. Time is advanced with a 3rd order mixed Backward Difference/Extrapolation (BDF3/EXT3) scheme. Along with its efficient parallelization, this code provides spectral accuracy with geometrical flexibility, which makes it suitable for some engineering problems.

The size of the computational domain is selected following El Khoury et al. (2013), who performed DNS of turbulent pipe flow (without heat transfer) also with Nek5000. The computational domain is shown in figure 1, and it consists of a circular pipe of length $25R$. Since the z direction is homogeneous, periodic boundary conditions are used in at the inlet and outlet of the pipe. The same computational mesh has been used for the three cases. We use a total of 55440 spectral elements of polynomial order $n = 7$, with 105 elements in the streamwise direction and 528 elements in the cross-plane. For cases 1 and 2, the grid spacing in wall units (i.e. normalised with u_τ and ν) is $\Delta r^+_{max} \leq 3.5$, $\Delta(R\theta)^+_{max} \leq 3.5$, $\Delta z^+_{min} \simeq 2.8$ and $\Delta z^+_{max} \leq 9$. The first grid point in the radial direction is located at $\Delta r^+ \simeq 0.25$ from the wall. Case 1 is well resolved, with a resolution slightly better than a similar case reported by El Khoury et al. (2013). The resolution for case 2 with $Pr = 4$ is slightly under-resolved compared to a channel flow computation with the same Reynolds number and $Pr = 3$ (Schwertfirm and Manhart, 2007).

The grid spacing for the more demanding simulation (case 3 in Table 1) is $\Delta r^+_{max} \leq 7$, $\Delta(R\theta)^+_{max} \leq 7$, $\Delta z^+_{min} \simeq 5.5$ and $\Delta z^+_{max} \leq 18$. The first grid point in the radial direction is located at $\Delta r^+ \simeq 0.5$ from the wall. This case is also

slightly under-resolved compared to the simulations reported by El Khoury et al. (2013).

The validation of the methodology was performed by carrying out an additional simulation with uniform heat flux, as the one reported by Piller (2005). The friction Reynolds number of the flow was set to $Re_\tau = 180$ and the Prandtl number to $Pr = 0.7$. The velocity statistics were compared to the DNS data of Wu and Moin (2008) and were found to be in good agreement (not shown). Details can be found in Gonzalo (2013). The mean temperature distribution $\langle T \rangle$ and the turbulent heat flux $\langle u_r' T' \rangle$ are displayed in Fig. 2. The data of Piller (2005) is included in the figure. Both calculations are shown to be in good agreement.

3. Results

3.1. Characterization of the temperature field

First, we provide a general impression of the velocity and temperature fields. Figure $3(a)$ shows a snapshot of the instantaneous streamwise velocity and Figure $3(b)$ displays a snapshot of the instantaneous temperature. Both plots correspond to case 3 with $Re_\tau = 360$ and $Pr = 0.7$. Note that, although the flow is turbulent in the whole pipe and velocity fluctuations are present everywhere, temperature fluctuations are concentrated in the upper part of the pipe. It can be observed that a thin thermal boundary layer develops in the upper region of the pipe where the heat flux is maximum. Near the adiabatic region the temperature distribution is more uniform.

A more quantitative view of the temperature is provided in Figures 4-6. First, Figure 4 displays the mean temperature $\langle T \rangle$ for the three cases, both as a contour plot in the cross-plane and as selected profiles. Also the mean temperature of the uniform heat-flux case (shown in Fig. 2) is included for comparison. The profiles are taken along three radial lines at $\theta = \pi/2, \pi/4$ and 0 as indicated in Figure $4(a)$. The distance to the pipe wall is plotted in wall units, $y^+ = (R - r)u_\tau/\nu$, using a logarithmic scale. The mean temperature in the contour plots is normalized with T^* so that the different thickness of the thermal boundary layers can be appreciated when comparing cases 1 and 2, that have the same Reynolds number. On the other hand, Figs. $4(d) - (f)$ show the deviation of the mean temperature with respect to the mean wall temperature $\langle T_w - T \rangle$, normalized with PrT^*. With this scaling all curves corresponding to the circumferentially-varying heat-flux cases collapse in the vicinity of the wall where the molecular conduction dominates over the turbulent heat diffusion.

One of the main concerns of the thermo-solar community is the temperature at wall, the so-called film temperature, since this is one of the main causes of pipe failure and salt degradation during operation. Figure 5 shows the variation of the wall temperature, $\langle T_w \rangle / T^*$, as a function of the circumferential coordinate. As expected, the maximum temperature is reached at the location of maximum heat flux, $\theta = \pi/2$, with a value which is slightly dependent on the Reynolds number but strongly affected by the Prandtl number. The comparison between cases 1 and

(a)

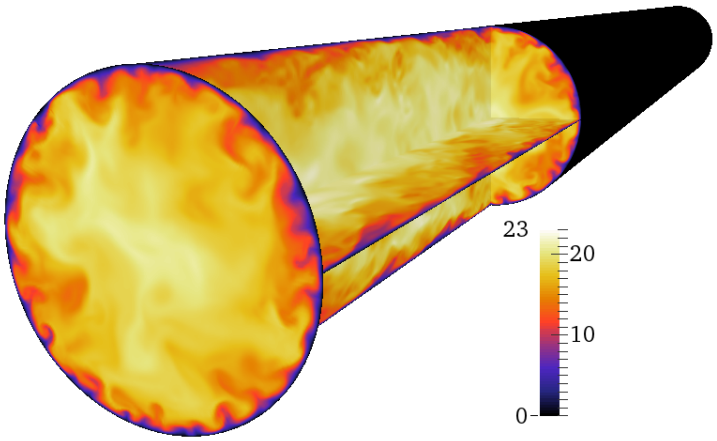

(b)

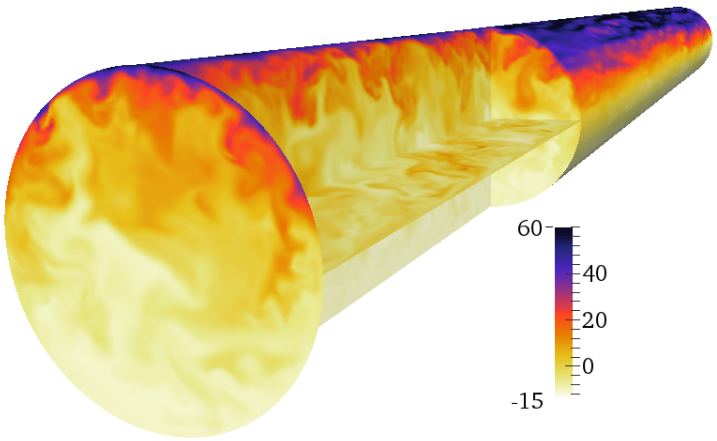

Figure 3: (a) Visualization of the instantaneous streamwise velocity, u_z/u_τ. (b) Visualizations of the instantaneous temperature T/T^*. Both visualizations correspond to Case 3 and are taken at the same time.

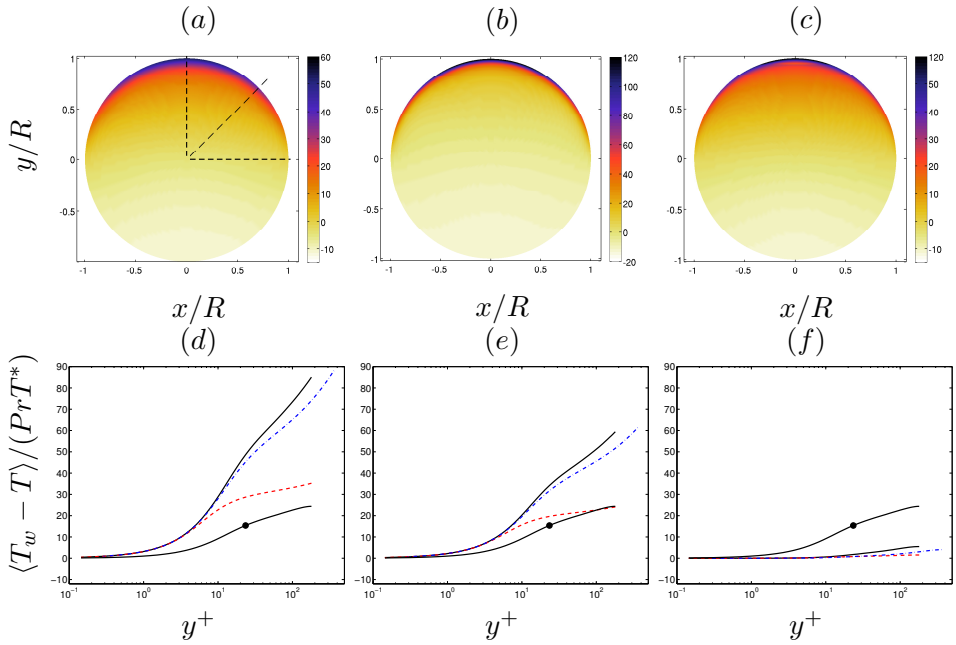

Figure 4: $(a)-(c)$ Mean temperature $\langle T\rangle/T^*$ in the cross-plane. Note that the scale is different in each panel. (a) Case 1. (b) Case 2. (c) Case 3. The dashed lines in (a) indicate the angles for which profiles are shown in $(d)-(f)$. $(d)-(f)$ Mean temperature, $\langle T_w - T\rangle/(PrT^*)$, profiles as a function of the distance to the wall y^+. Line styles defined in Table 1. The line with the symbol corresponds to the case with homogeneous heating. (d) $\theta = \pi/2$. (e) $\theta = \pi/4$. (f) $\theta = 0$.

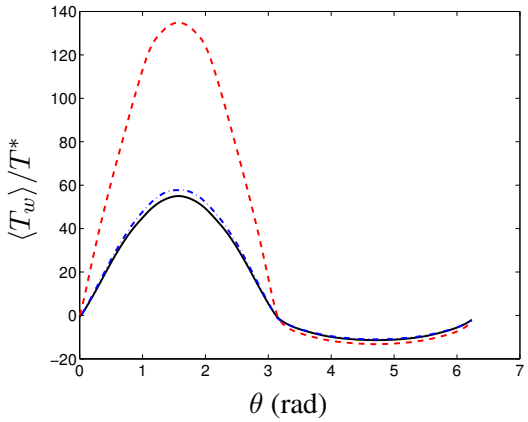

Figure 5: Mean temperature at the wall $\langle T_w \rangle / T^*$ as a function of the circumferential coordinate. Line styles defined in Table 1.

2 (with the same Reynolds number) suggests that the peak temperature changes as $\sqrt{Pr}$, although more simulations would be needed to confirm this trend.

The characterization of the temperature field is completed by analyzing the root-mean-square (RMS) temperature fluctuations. Figure 6 displays the RMS temperature fluctuations, T_{rms}, for the three cases, both as a contour plot in the cross-plane and as selected profiles. The profile of the RMS temperature fluctuations near the wall shows a plateau very close to the wall followed by a peak located at a distance to the wall that depends on the Prandtl number. After this peak the fluctuations decrease monotonically towards the center of the pipe. As shown in DNS of turbulent heat transfer in pipes (see for example Redjem-Saad et al. (2007)), when the Prandtl number increases, the peak of temperature fluctuations moves closer to the wall and rises significantly. The present results displayed in Figure 6(d) at $\theta = \pi/2$ show that for $Pr = 0.7$ the peak is located at $y^+ \simeq 11$, whilst for $Pr = 4$, this distance reduces up to $y^+ \simeq 7$. This difference is still clearly visible at $\theta = \pi/4$, Figure 6(e). At other circumferential locations where the heat flux at the wall vanishes, like in Figure 6(f), the temperature fluctuations are much weaker and the Pr effect is less apparent. We have tried several normalizations for the peak temperature fluctuations involving the Prandtl number with inconclusive results. Note that the scaling of thermal boundary layers is an issue of current debate even for canonical configurations (Saha et al., 2014).

3.2. Turbulent eddy diffusivity

The development of the fully developed thermal field in a turbulent pipe flow with a circumferentially-varying heat-flux is described by the three-dimensional mean energy equation

$$\langle u_z \rangle \frac{\partial T_b}{\partial z} = \frac{1}{r}\frac{\partial}{\partial r}\left[(\alpha + \varepsilon_{hr})\, r \frac{\partial \langle T \rangle}{\partial r}\right] + \frac{1}{r}\frac{\partial}{\partial \theta}\left[\frac{1}{r}(\alpha + \varepsilon_{h\theta})\frac{\partial \langle T \rangle}{\partial \theta}\right], \quad (5)$$

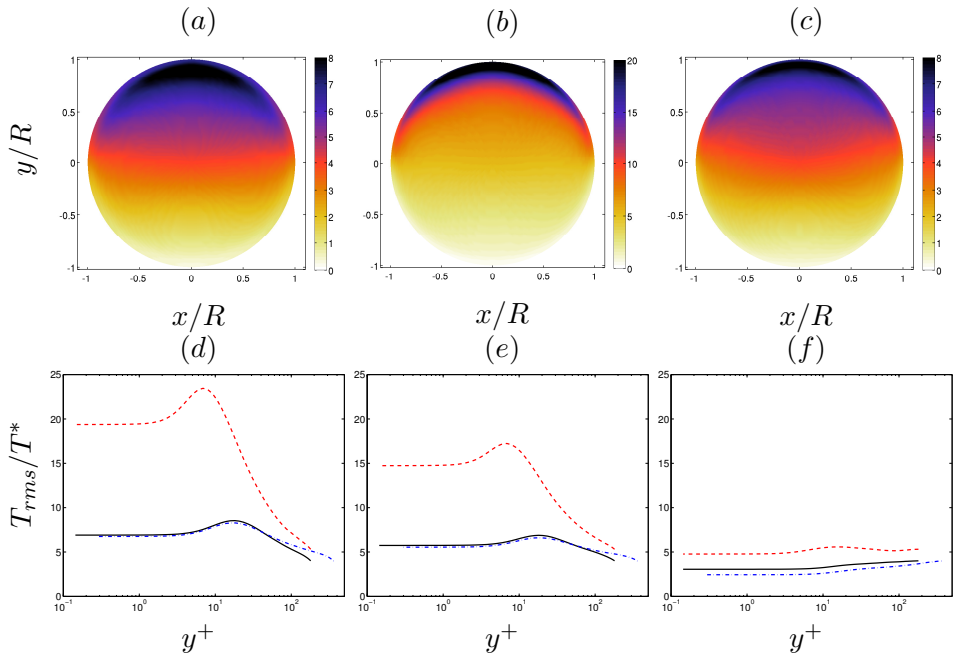

Figure 6: $(a) - (c)$ RMS temperature T_{rms}/T^* in the cross-plane. Note that the scale is different in each panel. (a) Case 1. (b) Case 2. (c) Case 3. $(d) - (f)$ RMS of temperature fluctuations, T_{rms}/T^*, profiles as a function of the distance to the wall y^+. Line styles defined in Table 1. (d) $\theta = \pi/2$. (e) $\theta = \pi/4$. (f) $\theta = 0$.

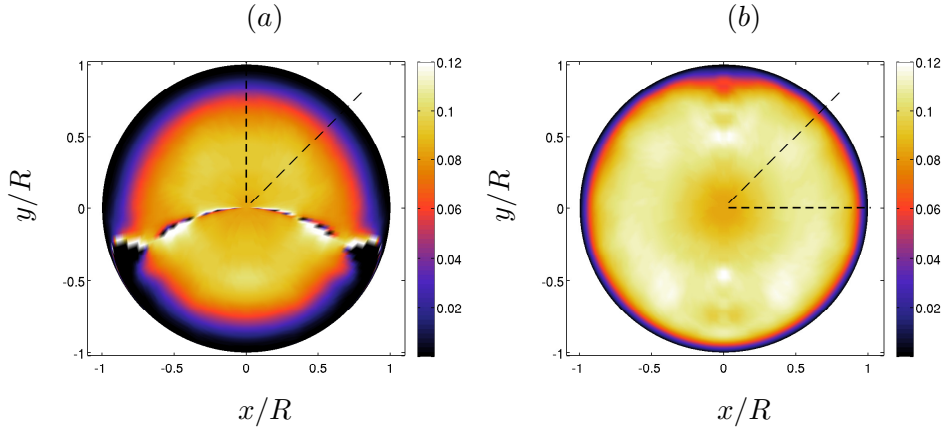

Figure 7: Thermal eddy diffusivity in (a) radial, $\varepsilon_{hr}/(u_\tau R)$, and (b) circumferential, $\varepsilon_{h\theta}/(u_\tau R)$, directions for Case 1. The dashed lines show the averaging region for Figure 8.

where we have introduced the eddy diffusivities to model the velocity-temperature correlations as

$$\left\langle u_r' T' \right\rangle = -\varepsilon_{hr} \frac{\partial \left\langle T \right\rangle}{\partial r}, \tag{6}$$

$$\left\langle u_\theta' T' \right\rangle = -\varepsilon_{h\theta} \frac{1}{r} \frac{\partial \left\langle T \right\rangle}{\partial \theta}. \tag{7}$$

Figure 7 shows the iso-contours obtained in the present DNS for the thermal eddy diffusitivies in radial, ε_{hr}, and circumferential, $\varepsilon_{h\theta}$, directions for Case 1. Although in principle these quantities could be a function of r and θ, the DNS results show that they are roughly functions of r only. Singularities appear in ε_{hr} when $\partial \left\langle T \right\rangle / \partial r$ goes to zero (near $\theta = 0$ and π). A singularity also occurs for $\varepsilon_{h\theta}$ at $\theta = \pi/2$ where $\partial \left\langle T \right\rangle / \partial \theta = 0$ at the wall. At this location $\varepsilon_{h\theta}$ seems to have circumferential variations, Figure $7(b)$. Although not shown here, the results for cases 2 and 3 are qualitatively similar.

In order to avoid the singularities, we have averaged ε_{hr} in the range $[\pi/4, \pi/2]$ and $\varepsilon_{h\theta}$ in the range $[0, \pi/4]$, as shown in Figure 7. The resulting eddy diffusivities normalized with $u_\tau R$ are shown in Figure 8, where the larger value of the thermal eddy diffusivity in the circumferential direction near the wall can be appreciated. Near the pipe center, both ε_{hr} and $\varepsilon_{h\theta}$ tend to the same values, indicating that the behaviour is rather isotropic. The value at pipe axis seems to be fairly independent of the Prandtl number with the present normalization.

As discussed in the introduction, we now proceed to evaluate the model proposed by Launder (1978). The eddy-diffusivity ratio $\varepsilon_{h\theta}/\varepsilon_{hr}$ is compared with the ratio of the corresponding mean square velocity fluctuations, $\langle u_\theta'^2 \rangle / \langle u_r'^2 \rangle$, both as a function of the distance to the wall in inner units (Figure 9). The present results indicate that both ratios differ near the wall. For $y^+ < 20$, the eddy diffusivity

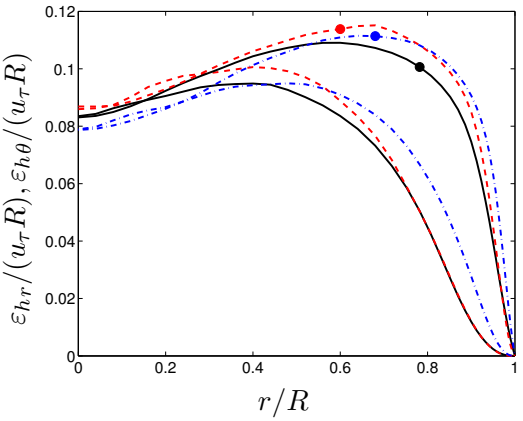

Figure 8: Thermal eddy diffusivity for both radial, $\varepsilon_{hr}/(u_\tau R)$ (without symbols), and circumferential, $\varepsilon_{h\theta}/(u_\tau R)$ (with symbols), directions as a function of the radial coordinate, r/R. Line styles defined in Table 1.

ratio is proportional to y^{-1} while the velocity ratio is proportional to y^{-2}. However, it seems that in the pipe core both ratios are of the same order of magnitude. A similar result was obtained in channel flow with heat flux varying in spanwise direction by Matsubara et al. (2012). Therefore, a non-isotropic eddy diffusivity model as proposed by Launder should be valid far from the wall. However, in order to provide the correct behaviour near the wall it should incorporate modifications with a proper scaling.

3.3. Turbulent Prandtl number

The knowledge of the turbulent Prandtl numbers is of great importance if we attempt to predict heat transfer from a known velocity field. We define turbulent Prandtl numbers in radial and circumferential directions

$$Pr_{tr} = \frac{\nu_t}{\varepsilon_{hr}}, \tag{8}$$

$$Pr_{t\theta} = \frac{\nu_t}{\varepsilon_{h\theta}}, \tag{9}$$

where ν_t is the eddy viscosity defined from

$$\left\langle u_r' u_z' \right\rangle = -\nu_t \frac{\partial \left\langle u_z \right\rangle}{\partial r}, \tag{10}$$

Note that in cases with uniform heating, the turbulent Prandtl number Pr_t corresponds to eq. (8).

In experiments, it is often difficult to determine the turbulent Prandtl number in turbulent boundary layer flows, since measurements near the wall are hard to obtain. With the advent of DNS, several authors have tried to address this problem, but mainly in cases with uniform heat transfer conditions. The behaviour of Pr_t

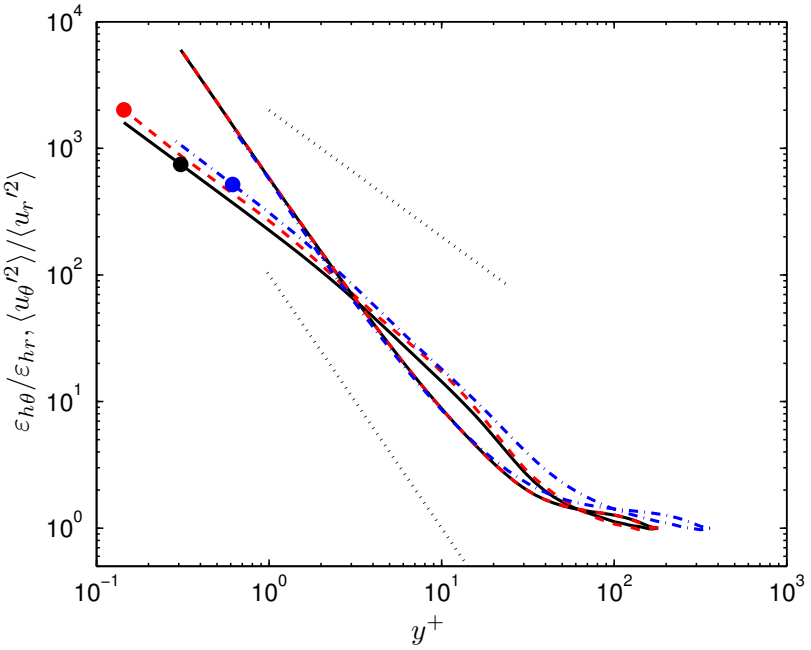

Figure 9: Ratio of thermal eddy diffusivities $\varepsilon_{h\theta}/\varepsilon_{hr}$ (with symbols), and ratio of velocity variances $\langle u_\theta{}'^2\rangle/\langle u_r{}'^2\rangle$ (without symbols) as a function of the distance to the wall, y^+. Line styles defined in Table 1. The dotted lines have slopes -1 and -2, respectively.

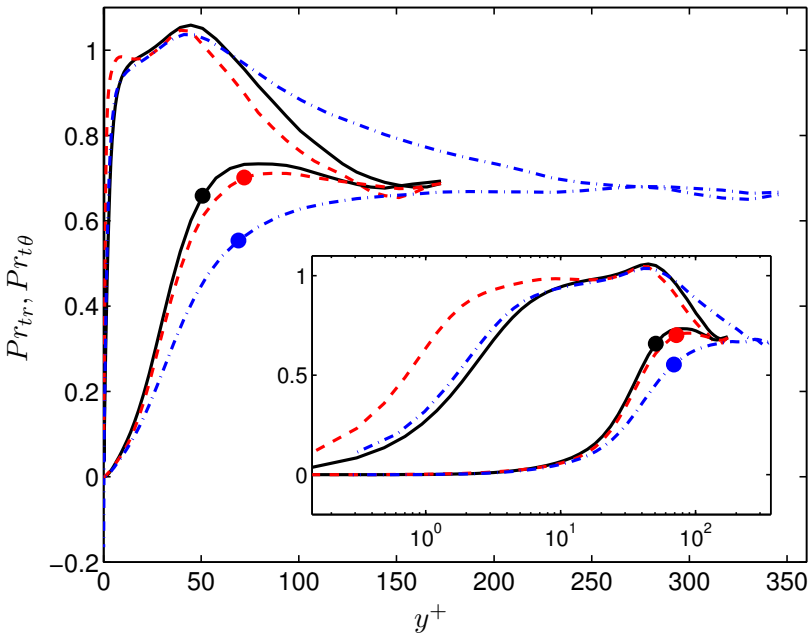

Figure 10: Turbulent Prandtl number for both radial, Pr_{tr} (without symbols), and circumferential, $Pr_{t\theta}$ (with symbols), directions as a function of the distance to the wall, y^+. Line styles defined in Table 1. The inset displays the same information as the main plot but the x-axis is shown in logarithmic scale.

near the wall is strongly dependent on the temperature boundary conditions. For isothermal walls (Schwertfirm and Manhart, 2007; Redjem-Saad et al., 2007) Pr_t tends to a finite value at the wall that depends on the molecular Pr. For constant heat flux at the wall Pr_t goes to zero at the wall (Chung and Sung, 2003). In the present case, where the heat flux conditions at the wall are non uniform, the characterization of the turbulent Prandtl number in the circumferential direction is of utmost importance.

Figure 10 shows Pr_{tr} and $Pr_{t\theta}$ for the three cases. As expected $Pr_{t\theta}$ is lower than Pr_{tr} in the near-wall region, indicating the higher contribution of the circumferential fluxes to the net turbulent heat transfer. As the distance to the wall approaches zero the circumferential turbulent Prandtl number is $Pr_{t\theta} \propto y^2$, while $Pr_{tr} \propto y$. In the buffer region, Pr_{tr} reaches values around 1 and then it decreases smoothly to reach a value $Pr_{tr} \sim 0.7$ in the central part of the pipe. On the other hand, $Pr_{t\theta}$ increases almost monotonically, and at the centre the temperature field becomes more isotropic, leading to $Pr_{t\theta} \sim Pr_{tr}$. At the pipe axis, the turbulent Prandtl numbers reaches a value of roughly 0.7 independently of the change in Re_τ and Pr, which agrees well with previous experimental data (Blackwell et al., 1972; Hollingsworth et al., 1989) and computations (Kim and Moin, 1989).

4. Conclusions

DNS of turbulent heat transfer of the fully-developed flow in a pipe with circumferentially-varying heat flux boundary conditions have been conducted for two Reynolds number ($Re_\tau = 180$ and 360) and two Prandtl numbers ($Pr = 0.7$ and 4). The imposed heat flux at the wall aims to reproduce the heat transfer conditions at the pipes of a heat receiver, therefore, the heat flux at the wall is modelled as sinusoidal from $\theta = 0$ to π and zero (adiabatic condition) from $\theta = \pi$ to 2π.

First, we focus on the mean and root-mean-square temperature distributions on the pipe cross-section. Most of the turbulent fluctuations take place in the upper part of the pipe where the heat flux is maximum. While the Reynolds number has a small impact on the wall temperature distribution, the Prandtl number produces deep changes, being the circumferential variations of temperature more pronounced when Pr is higher.

In orden to analyse the significance of the turbulent heat fluxes, thermal eddy-diffusivities are defined for the radial and circumferential directions similar to the definition of the eddy-viscosity in the momentum equation. Although in principle these quantities could be a function of r and θ, present DNS results show that they are roughly functions of r only. We found a similar ratio $\varepsilon_{h\theta}/\varepsilon_{hr}$ for all Re_τ and Pr cases studied, which varies as the inverse of the wall distance very near the wall. This implies that, although the Launder's hypothesis for the anisotropic behaviour might be valid far from the wall, the asymptotic behaviour of $\varepsilon_{h\theta}/\varepsilon_{hr}$ and $\langle u_\theta^2 \rangle / \langle u_r^2 \rangle$ differ near the wall, implying that a correction of the model is needed.

Finally, the turbulent Prandtl numbers for radial and circumferential directions relating the thermal eddy-diffusivities with the eddy-viscosity are presented and

discussed. At the center of the pipe, we obtain an isotropic behaviour with $Pr_{t\theta} \sim Pr_{tr} \sim 0.7$, irrespective of the Re and Pr considered here. Near the pipe wall, however, we find that $Pr_{tr} \propto y^{+}$ and $Pr_{t\theta} \propto y^{+2}$.

Acknowledgments

O.F. and M.G.-V. were partially supported by grant TRA2013-41103-P of the Spanish Ministry of Economy and Competitiveness. This grant includes FEDER funding. Fruitful discussions with Dr. C. Marugán-Cruz are gratefully acknowledged.

References

Baughn, J., Hoffman, M., Launder, B., Takahasi, R.K., 1984. J. Heat Transfer 106, 64–70.

Blackwell, B.F., Keys, W.M., Moffat, R.J., 1972. Report hmt-16. Thermosciences Division, Dept. Mech. Eng., Stanford Univ.

Chin, C., Monty, J., Ooi, A., 2014. Reynolds number effects in DNS of pipe flow and comparison with channels and boundary layers. Int. J. Heat Fluid Flow 45, 33–40.

Chung, S.Y., Sung, H.J., 2003. Direct numerical simulation of turbulent concentric annular pipe flow: Part 2: Heat transfer. Int. J. Heat Fluid Flow 24, 399–411.

El Khoury, G., Schlatter, P., Noorani, A., Fischer, P., Brethouwer, G., Johansson, A., 2013. Direct numerical simulation of turbulent pipe flow at moderately high Reynolds numbers. Flow, Turbul. Combust. 91, 475–495.

Fischer, P.F., Lottes, J.W., Kerkemeier, S.G., 2008. nek5000 Web page. Http://nek5000.mcs.anl.gov.

Flores, O., Marugán-Cruz, C., Santana, D., García-Villalba, M., 2014. Thermal stresses analysis of a circular tube in a central receiver. Energy Procedia 49C, 354–362.

Gärtner, D., Johannsen, K., Ramm, H., 1974. Turbulent heat transfer in a circular tube with circumferentially varying thermal boundary conditions. Int. J. Heat Mass Transfer 17, 1003–1018.

Gonzalo, A., 2013. Estudio numérico de transferencia de calor en conductos en régimen turbulento. Master's thesis. Univ. Carlos III de Madrid. Spain.

Hollingsworth, D.K., Keys, W.M., Moffat, R.J., 1989. Report hmt-41. Thermosciences Division, Dept. Mech. Eng., Stanford Univ.

Kim, J., Moin, P., 1989. Transport of passive scalars in a turbulent channel flow, in: Turbulent Shear Flows 6, pp. 85–96.

Kolb, G.J., 2011. An evaluation of possible next-generation high-temperature molten-salt power towers. Sandia National Labs, Report No. SAND2011-9320.

Launder, B.E., 1978. Heat and mass transport, in: P., B. (Ed.), Topics in Applied Physics. Turbulence.

Matsubara, K., Sakurai, A., Miura, T., Kawabata, T., 2012. Spanwise heat transport in turbulent channel flow with prandtl numbers ranging from 0.025 to 5. J. Heat Transfer 134, 041701.

Moore, S.R., Vernon, M., Ho, C.K., Siegel, N.P., Kolb, G.J., 2010. Design considerations for concentrating solar power tower systems employing molten salt. Sandia Report 6978.

Piller, M., 2005. Direct numerical simulation of turbulent forced convection in a pipe. Int. J. Numer. Meth. Fluids 49, 583–602.

Quarmby, A., Quirk, R., 1972. Measurements of the radial and tangential eddy diffusivities of heat and mass in turbulent flow in a plain tube. Int. J. Heat Mass Transfer 15, 2309–2327.

Redjem-Saad, L., Ould-Rouiss, M., Lauriat, D., 2007. Direct numerical simulation of turbulent heat transfer in pipe flows: effect of Prandtl number. Int. J. Heat Fluid Flow 28, 847–861.

Reynolds, W.C., 1963. Turbulent heat transfer in a circular tube with variable circumferential heat flux. Int. J. Heat Mass Transfer 6, 445–454.

Saha, S., Klewicki, J.C., Ooi, A.S.H., Blackburn, H.M., Wei, T., 2014. Scaling properties of the equation for passive scalar transport in wall-bounded turbulent flows. Int. J. Heat Mass Transfer 70, 779–792.

Schwertfirm, F., Manhart, M., 2007. DNS of passive scalar transport in turbulent channel flow at high Schmidt numbers. Int. J. Heat and Fluid Flow 28, 1204–1214.

Wu, X., Moin, P., 2008. A direct numerical simulation study on the mean velocity characteristics in turbulent pipe flow. J. Fluid Mech. 608, 81–112.